Chinese Journal of Aeronautics, 2013,26(4): 918–925

Chinese Society of Aeronautics and Astronautics
& Beihang University

Chinese Journal of Aeronautics

cja@buaa.edu.cn
www.sciencedirect.com

Numerical study of separation on the trailing edge of a symmetrical airfoil at a low Reynolds number

Lei Juanmian *, Guo Feng, Huang Can

School of Aerospace Engineering, Beijing Institute of Technology, Beijing 100081, China

Received 9 October 2012; revised 13 March 2013; accepted 27 April 2013
Available online 3 July 2013

KEYWORDS

Laminar separation bubble;
Low Reynolds number;
Simulation;
Symmetrical airfoil;
Trailing-edge separation

Abstract This study focuses on the trailing-edge separation of a symmetrical airfoil at a low Reynolds number. Finite volume method is adopted to solve the unsteady Reynolds-averaged Navier–Stokes (RANS) equation. Flow of the symmetrical airfoil SD8020 at a low Reynolds number has been simulated. Laminar separation bubble in the flow field of the airfoil is observed and process of unsteady bubble burst and vortex shedding from airfoil surfaces is investigated. The time-dependent lift coefficient is characteristic of periodic fluctuations and the lift curve varies nonlinearly with the attack of angle. Laminar separation occurs on both surfaces of airfoil at small angles of attack. With the increase of angle of attack, laminar separation occurs and then reattaches near the trailing edge on the upper surface of airfoil, which forms laminar separation bubble. When the attack of angle reaches certain value, the laminar separation bubble is unstable and produces two kinds of large scale vortex, i.e. primary vortex and secondary vortex. The periodic processes that include secondary vortex production, motion of secondary vortex and vortex shedding cause fluctuation of the lift coefficient. The periodic time varies with attack of angle. The secondary vortex is relatively stronger than the primary vortex, which means its influence is relatively stronger than the primary vortex.

1. Introduction

Low-Reynolds-number aerodynamics is very important for both military and civilian applications. Typical applications are wind turbines, remotely piloted vehicles, sailplanes, human powered vehicles, high altitude devices.[1–3] Recently, there is an increasing interest in the unmanned aerial vehicles (UAVs) and micro air vehicles (MAVs), which demands a deep and wide research on the aerodynamics of two-dimensional airfoils and three-dimensional wings.

It is well-known that many significant aerodynamics problems occur below chord Reynolds numbers of about 5×10^5. Compared to high Reynolds numbers, low Reynolds number aerodynamics is quite different. At high Reynolds numbers, the lift curve for airfoil is nearly linear with a slope of 2π. However, for low Reynolds numbers less than 5×10^5, the nonlinear features in the lift curve about 0° angle of attack (AOA) emerge for symmetrical airfoils; the maximum lift-to-drag ratio of airfoil deteriorates rapidly when the chord Reynolds numbers decrease in the vicinity of 5×10^5; besides, hysteresis

* Corresponding author. Tel.: +86 10 68912414.
E-mail address: leijm@bit.edu.cn (J. Lei).

Peer review under responsibility of Editorial Committee of CJA.

1000-9361
http://dx.doi.org/10.1016/j.cja.2013.06.005

can be seen in the lift characteristics of some airfoils at low Reynolds numbers.

Characteristics of laminar separation at low Reynolds numbers have been widely studied by analytical, experimental and computational methods for decades. From analytical and experimental aspects, Lissaman[4] gave a common review on the low Reynolds numbers airfoil aerodynamics from different perspectives such as the concept of low Reynolds numbers airfoil, fundamental fluid mechanics, experimental testing and theoretical design of airfoils. Horton[5] combined theoretical and experimental method to study the short type of bubble in two and/or three dimensional flow around airfoil and/or wing at low Reynolds numbers. He developed a semi-empirical theory for the prediction of the growth and bursting of two-dimensional short bubble and put an emphasis upon the conditions governing reattachment. Selig et al.[6,7] conducted tests on 34 different airfoils at low Reynolds numbers and acquired the lift and drag data of different airfoils at low Reynolds numbers. He analyzed the phenomena of the laminar separation bubble and its effects on the lift characteristics. He found a plateau in the lift curve of symmetrical airfoils in the vicinity of an angle of attack of 0° to be common in the *Re* range of 4×10^4 to 1×10^5. He also found hysteresis loops in the lift curve for some airfoils and considered whether counterclockwise or clockwise hysteresis loop can occur for a given *Re*. Yang et al.[8] conducted an experimental study on the aerodynamic characteristics of GA (W)-1 airfoil and investigated the aerodynamic hysteresis of airfoil at a low Reynolds number. Mueller and Batill[9] investigated the separation on a two-dimensional NACA66-018 airfoil using smoke visualization method and classified it as the leading-edge separation bubble. From simulation aspects, Refs. [10,11] simulated the flow around a two-dimensional airfoil and observed periodic vortex shedding. Lee et al.[12] classified airfoils according to the type of pattern shown by its corresponding lift coefficient curve and explained the reasons contributing to the abnormal behavior of the lift curves for various airfoils using computational fluid dynamics (CFD). Bai et al.[13,14] conducted a simulation on the flow around symmetrical and non-symmetrical airfoil at low Reynolds number and proposed a trailing-edge separation bubble model. He applied the model to explain the aerodynamic characteristics of the symmetrical airfoil at small angle of attack under low *Re* and mechanism of the nonlinear effect in the lift curve at small angle of attack. Ye et al.[15,16] carried out a direct numerical simulation (DNS) on the separation mechanism of two-dimensional airfoil and described the rules of vortex interaction. Zhang and Yang[17] simulated the unsteady two-dimensional low Reynolds number flow over Epper387 airfoil with an unsteady RANS solver and the transition point is fixed for different turbulence models. He also analyzed the effect of transition on the low-Reynolds-number flow. Sheng[18] discussed the characteristics of four types of airfoils with analytical, computational and experimental method and gave some suggestions on the shapes of airfoils at low Reynolds numbers. The present paper conducts a numerical simulation on the flow around a symmetrical SD8020 airfoil and studied the trailing-edge separation bubble mechanism by analyzing the flow field structure and surface pressure distribution. The shedding process of the vortex of the symmetrical airfoil is analyzed and the pattern of vortex shedding is also given.

2. Computation scheme

2.1. Governing equation

For the two-dimentional, unsteady and incompressible flow, we consider that the governing equations are the RANS equations without the gravity and the body force items in Cartesian tensor form:

$$\begin{cases} \frac{\partial u_i}{\partial x_i}=0 \\ \frac{\partial u_i}{\partial t}+u_j\frac{\partial u_i}{\partial x_j}=-\frac{1}{\rho}\frac{\partial p}{\partial x_i}+\nu\frac{\partial^2 u_i}{\partial x_j\partial x_j}-\frac{\partial\overline{u_i'u_j'}}{\partial x_j} \end{cases} \tag{1}$$

where u_i is the mean velocity, ν the kinematic viscosity of the air, ρ the density of air, p the pressure, and $-\overline{u_i'u_j'}$ the Reynolds stress.

2.2. Turbulence model

The shear stress transport (SST) k-ω turbulence model[19] is a two-equation turbulence model which can precisely predict adverse pressure gradient flows and airfoil flows. It effectively combines the robust and accurate formulation of the k-ω model in the near-wall region with the free-stream independence of the k-ε model in the far field.

$$\begin{cases} \frac{\partial}{\partial t}(\rho k)+\frac{\partial}{\partial x_i}(\rho k u_i)=\frac{\partial}{\partial x_j}(\Gamma_k\frac{\partial k}{\partial x_j})+\widetilde{G_k}-Y_k \\ \frac{\partial}{\partial t}(\rho\omega)+\frac{\partial}{\partial x_i}(\rho\omega u_i)=\frac{\partial}{\partial x_j}\left(\Gamma_\omega\frac{\partial\omega}{\partial x_j}\right)+G_\omega-Y_\omega+D_\omega \end{cases} \tag{2}$$

where $\widetilde{G_k}$ represents the generation of turbulence kinetic energy due to mean velocity gradients and G_ω the generation of ω, Γ_k and Γ_ω represent the effective diffusivity of k and ω, respectively, Y_k and Y_ω represent the dissipation of k and ω due to turbulence, D_ω represents the cross-diffusion term.

In order to simulate transition from laminar to turbulence, a low-Reynolds-number correction is used by which three closure coefficients α^*, α, β^* are added to the turbulent viscosity μ_t, G_ω and Y_k when the k-ω model is activated in the near-wall region.

$$\mu_t=\alpha^*\rho k/\omega \tag{3}$$

$$G_\omega=\alpha\frac{\omega}{k}\cdot\tau_{ij}\frac{\partial u_j}{\partial x_j} \tag{4}$$

$$Y_k=\rho\beta^* k\omega \tag{5}$$

For detailed information about the low-Reynolds number correction method in the k-ω model, readers can refer to Ref. [20].

2.3. Model, grid and boundary conditions

The present paper conducts a simulation on the flow around the SD8020 airfoil. The model and the established Cartesian coordinate are shown in Fig. 1(a). The airfoil is symmetrical and smooth, with its chord length c = 0.3048 m.

A C-type mesh generated by elliptical method is adopted to discrete the flow field of the airfoil. The C-type grid constitutes 82000 nodes with 290 grid points on the airfoil surface and the external computational boundaries are set to be $20c$ from the airfoil. The partial mesh of the domain is shown in Fig. 1(b). The height of the first row of the cells bounding the airfoil is

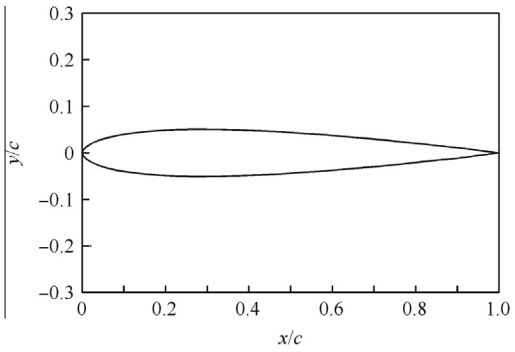

(a) Schematic of SD8020 airfoil geometry and the coordinates

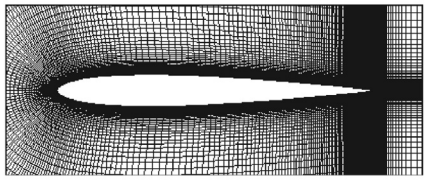

(b) Schematic of the partial domain of SD8020

Fig. 1 Schematic of the model geometry and partial domain of SD8020 airfoil.

set to be 0.0001 which ensures $y^+ \leqslant 1$. The time step size is 0.0001 s and the turbulence intensity of free stream is 0.1%. The boundary conditions in the present paper are: (A) the upstream and lower boundary adopt the velocity-inlet boundary, i.e. given the value of velocity; (B) the downstream and upper boundary adopt pressure-outlet boundary; (C) the model surface adopt the wall boundary.

3. Presentation of result

3.1. Characteristics of lift curve

The simulated range of angle of attack in the paper is from -4° to 10°. The time-dependent lift coefficient during the unsteady simulation at different angles of attack at $Re = 4 \times 10^4$ is shown in Fig. 2. For the symmetrical airfoil at low Re, periodical fluctuations of the time-dependent lift coefficient C_L can be seen from Fig. 2 and the amplitude of fluctuations is increasing with the angle of attack.

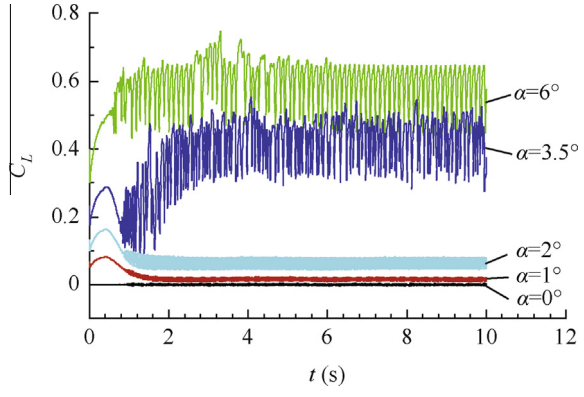

Fig. 2 History of lift coefficient at different AOA ($Re = 4 \times 10^4$).

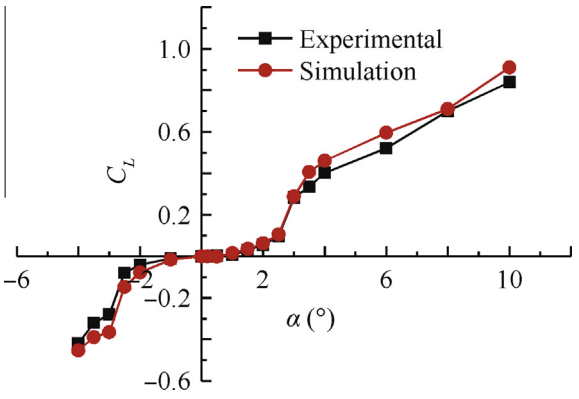

Fig. 3 Time-averaged lift coefficient at different AOA ($Re = 4 \times 10^4$).

Fig. 3 shows the time-averaged lift coefficient compared to the experiments by Selig et al.[6] at different angles of attack at $Re = 4 \times 10^4$. The simulation results agree well with the experiment, which validates the simulation method's accuracy. A plateau in the lift curve in the range from -1° to 1° emerges and the curve slope is obviously lower than 2π; from angle of attack of 1.5° to 2.0°, the curve slope begins to increase; from angle of attack of 2.5° to 3.5°, the curve slope reaches the maximum and is obviously more than 2π; after the angle of attack reaches 4.0°, the curve slope resumes the typical linear characteristic.

3.2. Time-averaged results and the mechanism for laminar separation bubble (LSB)

Fig. 4 shows the surface pressure coefficient C_p distribution of the symmetrical SD8020 airfoil at angles of attack of 0°, 0.5°, 1.5°, 2.0°, 2.5°, 3.0°, 4.0°, 6.0° at $Re = 4 \times 10^4$, in which Wallup and Walldown respectively represent the upper and lower surface of airfoil. From Fig. 4 we can see that before angle of attack α less than 2.0°, the pressure distribution curve is smooth and no oscillation emerges; when the α equals 2.5°, oscillation is observed in the pressure curve along the trailing edge of the upper surface of airfoil. With the increase of the AOA, while the onset of oscillation of the pressure curve along the upper trailing edge moves forward and the area and amplitude are both turning larger, the pressure curve of the lower surface of airfoil still remains smooth.

Fig. 5 shows the time-averaged streamlines of the symmetrical SD8020 airfoil at angles of attack of 0°, 0.5°, 1.5°, 2.0°, 2.5°, 3.0°, 4.0°, 6.0° at $Re = 4 \times 10^4$. From Fig. 5 we can see that for the symmetrical SD8020 airfoil at $Re = 4 \times 10^4$, flow separation occurs on both surfaces of airfoil at 0° and other small AOAs. This is because, for low Reynolds number flow, fluid viscosity effect plays a predominant role which results in "boundary layers" growing rapidly and separating from the surfaces of the airfoils easily. Those factors which affect boundary layer separation and transition in the boundary layer are fluid viscosity and adverse pressure gradient in the boundary layer. The boundary layer on the airfoil often remains laminar on the leading edge of the upper surface of airfoil. When the boundary layer travels far enough against the adverse pressure gradient, the speed of the boundary layer falls almost to zero. This detaches the flow from the surface of the

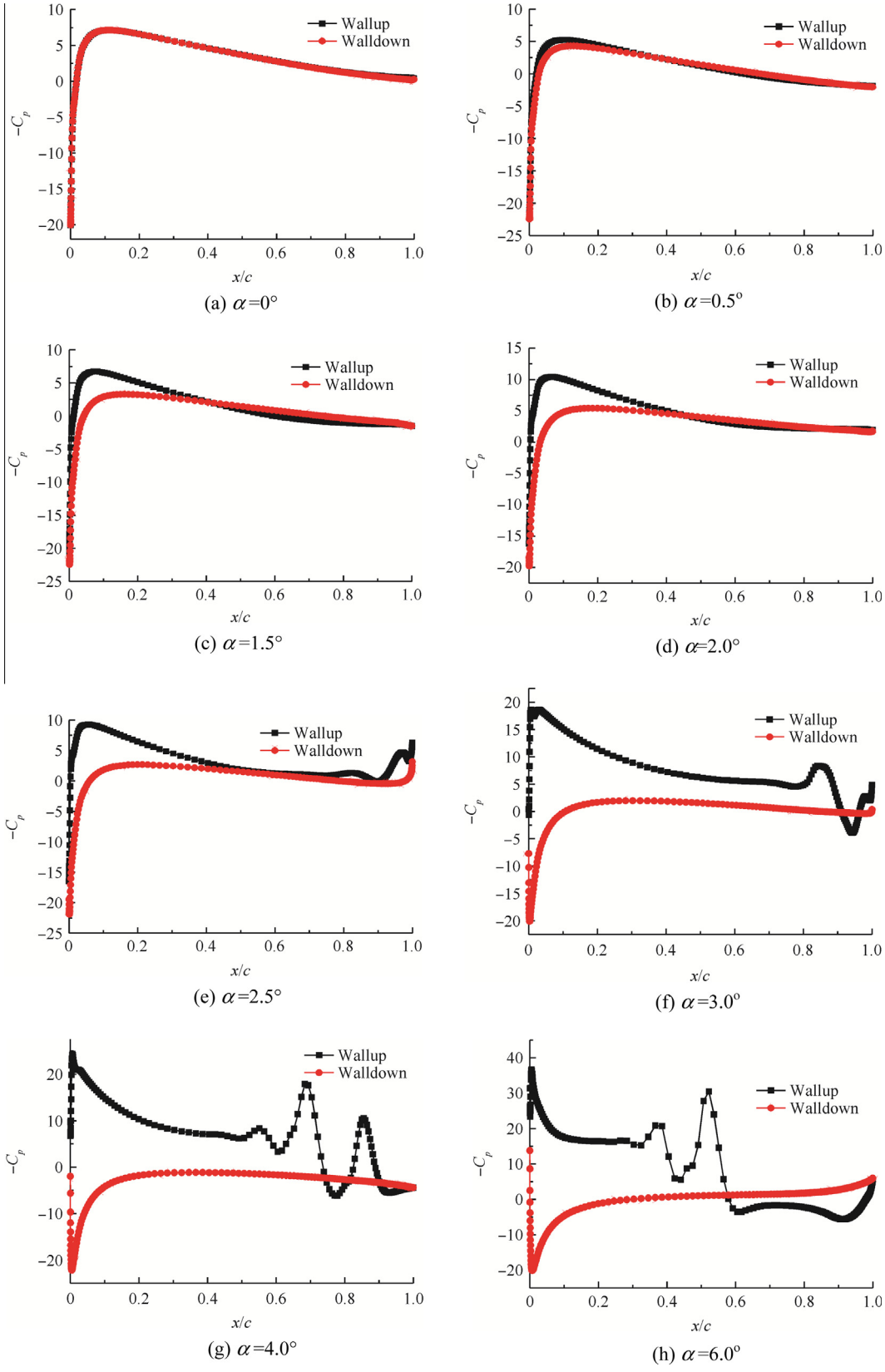

Fig. 4 Surface pressure distribution at different AOAs ($Re = 4 \times 10^4$).

airfoil. This can be verified from Fig. 4 which shows that most of the upper surface of airfoil is in adverse pressure gradient. Under the influence of adverse pressure gradient combined with viscosity, the speed of the boundary layer falls almost to zero until separation occurs on the trailing edge of the upper surface.

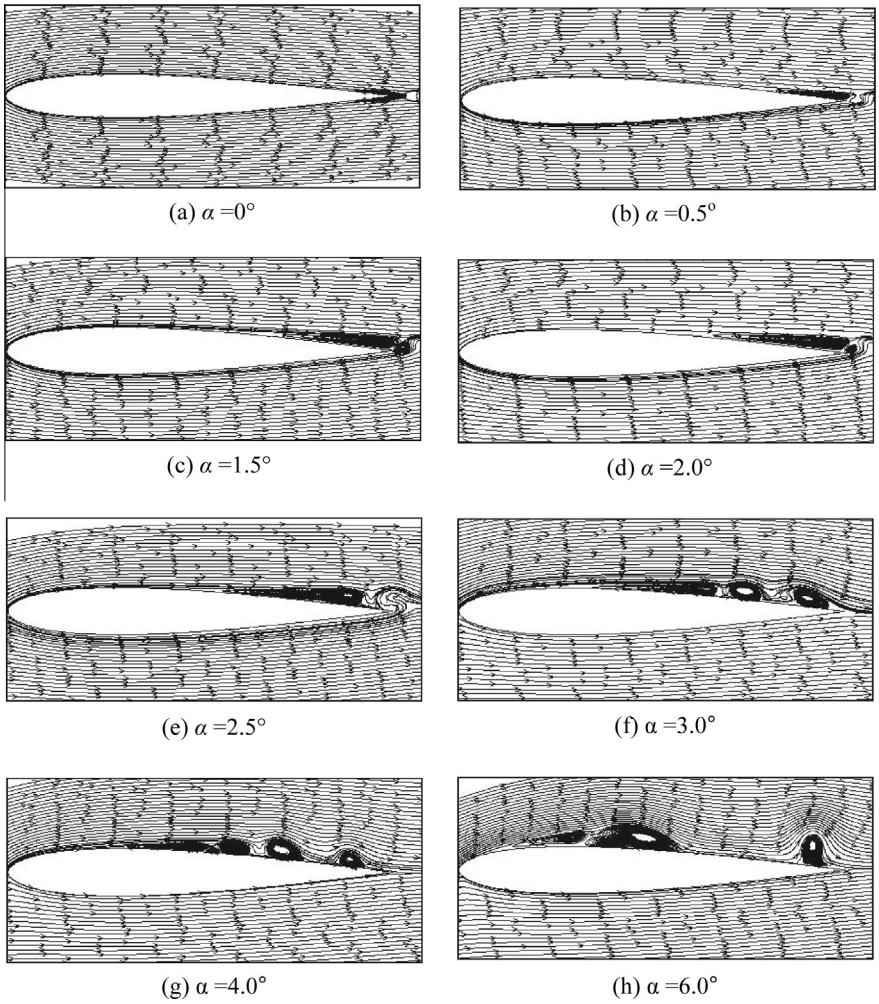

Fig. 5 Time-averaged streamlines at different AOAs ($Re = 4 \times 10^4$).

From Fig. 5, for $\alpha = 0°$, laminar separation can be seen on the trailing edge of both surfaces of airfoil. When AOA is less than 2°, with the increase of AOA, the separation point on the upper surface of airfoil gradually moves forward, while the separation on the lower surface of airfoil gradually moves backward until no separation occurs. Combined with Fig. 4 we can conclude that changes in the separation region have little effect on the surface pressure distribution of the upper surface. From the view of flow structure, as Fig. 5 shows, the effective shape of the symmetrical airfoil has changed under the effect of laminar separation. The rear stagnation point of the flow moves from the trailing edge to the aft-top of the airfoil, which equals flow around a negative-cambered airfoil. With the AOA increasing, the negative camber of equivalent airfoil turns larger. The combined action of both negative airfoil camber and the AOA results in little change in the lift before AOA reaches to 2°, even a plateau in the lift curve emerges from AOA of −1° to 1°. When the AOA is in the range from 2.5° to 3.5°, the separation point on the upper surface goes on moving forward with the AOA increasing and the separation region turns larger. From Fig. 5(f), we can see that the separated flow on the upper surface starts to reattach which forms what is called laminar separation bubble on the trailing edge of the upper surface. This causes a sudden increase of the lift-curve slope.

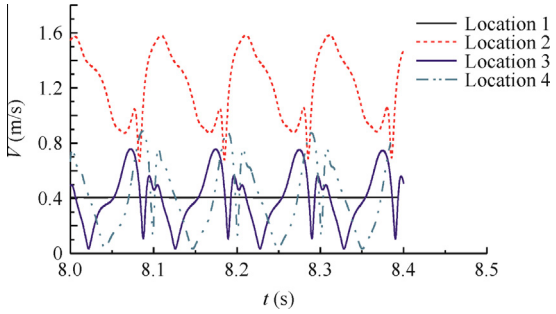

Fig. 6 History of the velocity V.

Fig. 6 shows the history of the velocity V at different points which are located in the boundary layer along the upper surface of SD8020 airfoil of $\alpha = 3°$ at $Re = 4 \times 10^4$. The point Location 1 is located at the leading edge and its coordinate is $(x, y) = (0.0054, 0.0055)$. The points, i.e. Location 2, Location 3, Location 4, are all located at the trailing edge and their coordinates are

respectively $(x, y) = (0.2600, 0.0120)$, $(x, y) = (0.2750, 0.0036)$, $(x, y) = (0.2800, 0.0031)$.

From Fig. 6 we can conclude that the separated shear layer is very unstable and normal velocity disturbances are quite strong, which demonstrates it turns into turbulent flow. The turbulent shear stresses energize the separated shear layer by entraining fluid from the external stream. Reattachment occurs as a turbulent boundary layer when the separated shear layer is able to overcome the adverse pressure gradient. This forms what is called laminar separation bubble. The turbulent is able to overcome adverse pressure gradient and travels along the surface until it leaves from the upper trailing edge. The vortexes in Fig. 5(f) are the primary separation bubble and the vortexes produced by the primary bubble. Detailed analysis will be discussed in the following part.

As the AOA continues to increase, the flow pattern remains unchanged until stall; the separation bubble continues to move forward. So in terms of the trailing-edge separation, details in the present paper will be discussed in the case of $\alpha = 3.0°$.

3.3. Analysis of periodical flow

Through the periodical variation of the flow structure, the periodical cycles can be achieved and correspond well with the subtraction between the two adjacent peak values in the lift curve. For example, at $\alpha = 3°$, the periodical cycle for vortex shedding is about 0.068 s. Table 1 shows the vortex shedding cycle at different AOAs.

From Table 1 we can see that for symmetrical SD8020 airfoil at $Re = 4 \times 10^4$, the vortex shedding cycle varies with AOA. As the AOA increases, the vortex shedding cycle increases. This is because with the increase of the AOA, the location of LSB on the upper surface of airfoil constantly moves forward, which causes the distance of the vortex traveling to the trailing edge to turn bigger and the motion time to become longer. At $\alpha = 3°$, the streamline for the symmetrical SD8020 airfoil at different moments but in one cycle is shown in Fig. 7. From Fig. 7 we can see that the flow in the boundary layer is featured by strong unsteadiness since there are complex vortex structures on the upper surface. These large-scale vortexes can be classified into two kinds: the primary vortex and the secondary vortex. The primary vortex is located in the vicinity of separation point and is constrained by the wall and the free stream. It is wedge-shaped and its structure is relatively stable. The major function of primary vortex is entraining fluid with higher momentum from the external stream. In the process of spatial evolution, the head of primary vortex is gradually stretched under the shear action of external stream until the primary vortex is split and produces a secondary vortex. The secondary vortex is produced by the primary vortex and it gradually grows through entraining energy from external stream and then sheds apart from the primary vortex. Finally, under the action of external stream and wall, the secondary vortex moves along the upper trailing edge until it sheds from the trailing edge.

Table 1 Vortex shedding cycle on upper surface ($Re = 4 \times 10^4$).

α (°)	2.5	3.0	4.0	6.0
Vortex shedding cycle T (s)	0.044	0.068	0.068	0.122

As can be seen in Fig. 7(a), at the moment of $t = \frac{1}{18}T$, there exists both the primary vortex and the secondary vortex. With time advancing, the primary vortex is stretched and the secondary vortex is moving to the trailing edge. From Fig. 7(d), i.e. at the moment of $t = \frac{8}{18}T$, under the effect of wall and external stream and the secondary vortex, the primary vortex is stretched to the maximum while the previous secondary vortex has moved to the vicinity of the upper trailing edge. From Fig. 7(g), i.e. at the moment of $t = \frac{14}{18}T$, a new secondary vortex is produced by the primary vortex while the previous secondary vortex is about to shed from the upper trailing edge. As to Figs. 7(h) and 7(i), with the time advancing, the primary vortex is stretched under the effect of external stream, the wall and the secondary vortex, and the new produced secondary vortex moves to the upper trailing edge, while the previous secondary vortex has shed from the upper surface of airfoil. So back and forth, the periodical variation of LSB on the upper trailing edge arouses the non-linear effect and periodical oscillation of the lift curve of symmetrical airfoil under low Re.

As can be seen from the previous Fig. 4, the pressure distribution at the vortex location on the upper surface is smooth without sudden changes. However, a sudden change occurs at the oscillating area of the pressure curve. Combined with Fig. 7, we can see that the location of secondary vortex corresponds well with the oscillating area of the pressure curve while the location of primary vortex corresponds with the smooth part of the pressure curve. This turns out that the intensity of primary vortex is weaker imposing less effect on the upper surface pressure distribution, while the intensity of secondary vortex is stronger which has a greater impact on the upper surface pressure distribution. The reason for the difference of intensity between the primary vortex and secondary vortex may be that the relatively stable primary vortex has less energy exchange with the external stream, so the intensity of the primary vortex is weaker and its effect on the aerodynamic characteristics is smaller. However, the secondary vortex is constantly moving and shedding and has greater energy exchange with the external stream. So the intensity of secondary vortex is higher and has a greater impact on the aerodynamic characteristics.

4. Conclusions

(1) At low Reynolds number, there exist oscillations in the time dependent lift coefficient curve for the symmetrical SD8020 airfoil and the non-linear feature exists in the lift curve at 0° angle of attack.
(2) At low Reynolds number, laminar separation occurs on both surfaces of airfoil at small angle of attack. As the AOA increases, laminar separation bubbles emerge on the upper trailing edge of airfoil and they are periodical burst and shedding. The vortex shedding cycles vary with the angle of attack: the higher the AOA, the longer the vortex shedding cycle.

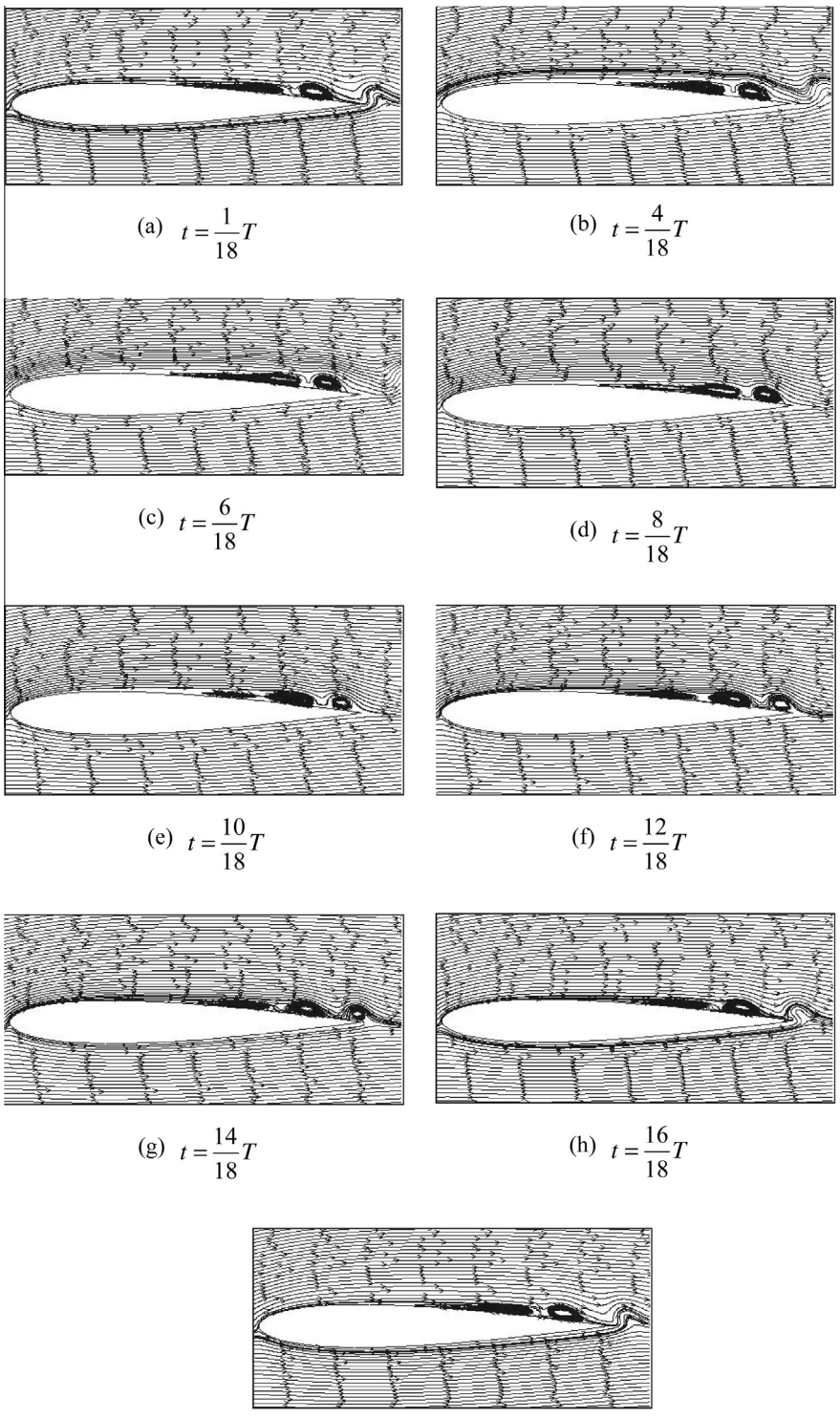

Fig. 7 Streamlines for SD8020 airfoil ($Re = 4\times10^4$, $\alpha = 3.0°$).

(3) At low Reynolds number, when the AOA reaches a certain value, the separation bubble on the upper trailing edge in the flow field of airfoil is unsteady and produces two kinds of large-scale vortex, the primary vortex and the secondary vortex.

(4) The periodical processes including the primary vortex producing the secondary vortex, the motion of the secondary vortex and the periodical shedding for the secondary vortex from the surface of airfoil cause the oscillation of aerodynamic characteristics.

(5) The intensity of primary vortex is weaker and imposes less effect on the upper surface pressure distribution, while the intensity of secondary vortex is stronger which has a greater impact on the upper surface pressure distribution.

References

1. Yang ZF, Fred LH, Hu H. An experimental investigation on the flow separation on a low-Reynolds-number airfoil. *45th AIAA aerospace sciences meeting and exhibit*; 2007.
2. Mueller TJ, DeLaurier JD. Aerodynamics of small vehicles. *Annu Rev Fluid Mech* 2003;**35**(1):89–111.
3. Carmichael BH. Low Reynolds number airfoil survey. California: Low Energy Transport systems; 1981. Report No.: NASA-CR-165803-Vol-1.
4. Lissaman PBS. Low-Reynolds-number airfoils. *Annu Rev Fluid Mech* 1983;**15**(1):223–39.
5. Horton HP. *Laminar separation bubbles in two and three dimensional incompressible flow* [dissertation]. London: University of London; 1968.
6. Selig MS, Guglielmo JJ, Broern AP, Giguère P. Experiments on airfoils at low Reynolds numbers. In: *34th AIAA aerospace sciences meeting and exhibit*; 1996.
7. Selig MS, Guelielmo JJ, Broeren AP, Giguère P. *Summary of low-speed airfoil data*. Virginia: SoarTech Publications; 1995.
8. Yang ZF, Igarashi H, Martin M, Hu H. An experimental investigation on aerodynamic hysteresis of a low Reynolds number airfoil. In: *46th AIAA aerospace sciences meeting and exhibit*; 2008.
9. Mueller TJ, Batill SM. Experimental studies of separation on a two-dimensional airfoil at low Reynolds numbers. *AIAA J* 1982;**20**(4):457–63.
10. Pauley LL, Moin P, Reynolds WC. The structure of two-dimensional separation. *J Fluid Mech* 1990;**220**:397–411.
11. Lin JCM, Pauley LL. Unsteady laminar separation on low Reynolds number airfoils. In: *31st AIAA aerospace sciences meeting & exhibit*; 1993.
12. Lee CS, Pang WW, Srigrarom S, Wang DB, Hsiao FB. Classification of airfoils by abnormal behavior of lift curves at low Reynolds number. In: *24th AIAA applied serodynamics conference*; 2006.
13. Bai P, Cui EJ, Li F, Zhou WJ. Study of the nonlinear lift coefficient of the symmetrical airfoil at low Reynolds number near the 0° angle of attack. *Chin J Theor Appl Mech* 2006;**38**(1):1–8 [Chinese].
14. Bai P, Cui EJ, Zhou WJ. Numerical simulation of laminar separation bubble over 2D airfoil at low Reynolds number. *Acta Aerodyn Sin* 2006;**24**(4):416–24 [Chinese].
15. Ye J, Zou ZP, Lu LP, Yang L. Investigation of separation mechanism for airfoil leading edge flow at low Reynolds number. *J Beijing Univ Aeronaut Astronaut* 2004;**30**(8):693–7 [Chinese].
16. Ye J, Lin GH, Zou ZP, Lu LP. The analysis of flow around a 2D airfoil at low Reynolds number. *J Aerosp Power* 2003;**18**(1):38–45 [Chinese].
17. Zhang Q, Yang Y. Numerical analysis of low Reynolds number flow over airfoil. *Acta Aerodyn Sin* 2006;**24**(4):482–6 [Chinese].
18. Sheng YH. *A study of low-Reynolds-number performance over a two-dimensional airfoil for micro-air vehicle* [dissertation]. Nanjing: Nanjing University of Aeronautics and Astronautics; 2003 [Chinese].
19. Menter FR. Two-equation eddy-viscosity turbulence models for engineering applications. *AIAA J* 1994;**32**(8):1598–605.
20. Wilcox DC. Simulation of transition with a two equation turbulence model. *AIAA J* 1994;**32**(2):247–55.

Lei Juanmian is an associate professor at School of Aerospace Engineering, Beijing Institute of Technology, Beijing, China. She received B.S. degree from Northwestern Polytechnical University in 1991 and Ph.D. degree from Beijing Institute of Technology in 2001. Her current research interests are flying vehicle aerodynamic configuration design and complex flow numerical simulation.